Superconducting wigglers and undulators : technical aspects

Mezentsev Nikolay

Budker institute of Nuclear Physics,
Novosibirsk, Russia

Contents

- Introduction
- History
- Superconducting materials
- SC coil design types for multipole wigglers and undulators
- SC ID field calculations
- Transition of superconductor to normal state. (Quench)
- Quench detection and quench protection
- Influence of SC ID field on beam dynamics
- SC ID cryogenic systems
- Current feeding of SC ID
- SC ID magnetic measurements systems

Superconductivity phenomena -100 years

The phenomenon of superconductivity was discovered in 1911 by the Dutch physicist H. Kamerlingh Onnes and his assistant Gilles Holst in Leiden. They found that *dc resistivity of mercury suddenly drops to zero below 4.2 K.*

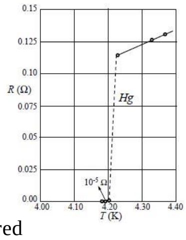

In 1933, W. Meissner and R. Ochsenfeld discovered in Berlin one of the most fundamental properties of superconductors: *perfect diamagnetism.*

The first microscopic theory of superconductivity in metals was formulated by J. Bardeen, L. Cooper and R. Schrieffer in 1957, which is now known as the *BCS theory.*

Introduction

Superconducting (SC) wigglers (SCWs) and undulators (SCUs) are high performance IDs suitable for extending the spectral range of SR storage rings towards shorter wavelengths and harder x-rays, increase brightness of photon sources. The SCWs can be either wave length shifters (WLS) with a few magnet poles with very high magnetic field or multipole wigglers (MPW) with a large number of poles with high magnetic field. The maximum magnetic field in SCWs and SCUs is defined by the critical curve of the SC wire. SC MPWs fabricated with use of Nb-Ti/Cu wire provide magnetic fields that are 2-3 times higher than what can be obtained using permanent magnets for the same pole gap and period length. SCWs and SCUs, as a rule, have zero first and second magnetic field integrals along electron orbit and their operation does not affect the working reliability of the storage ring.

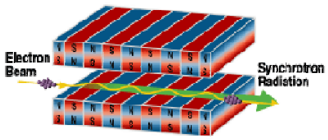

There is no any basic difference between wiggler and undulator. Phase errors in a magnetic field are more important for undulators as spectrum-angular properties of radiation are formed by all undulator length.

The main parameter of alternating-sign magnetic field which defines radiation property is K-value:

$$K = 0.934 \cdot l_0[\mathrm{cm}] B_0[\mathrm{T}]$$

K~1 - undulator.
K>>1 - wiggler

History

First superconducting multipole wiggler, BINP, Russia

The history of SC IDs used for generation of SR started more than 30 years ago in Budker INP where the first SC MPW was designed and fabricated in 1979. The first SC MPW was installed on the 2 GeV storage ring VEPP-3 to increase photon flux density with higher energy. The cross section of the vacuum chamber of the SCW was like a keyhole where a wide vertical area was used for injection (30 mm), and narrow area (8 mm) was used for creation of magnetic field by the wiggler. These two areas were connected by narrow 5.5 mm slit for electron beam moving from injection area to area with high magnetic field. In order to move the electron orbit from the injection area to the working area, 4 steering magnets were used.

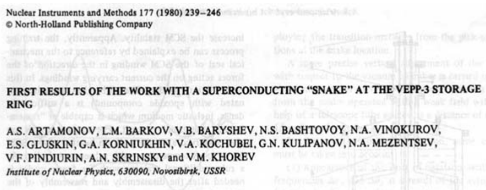
Nuclear Instruments and Methods 177 (1980) 239–246

FIRST RESULTS OF THE WORK WITH A SUPERCONDUCTING "SNAKE" AT THE VEPP-3 STORAGE RING

A.S. ARTAMONOV, L.M. BARKOV, V.B. BARYSHEV, N.S. BASHTOVOY, N.A. VINOKUROV, E.S. GLUSKIN, G.A. KORNIUKHIN, V.A. KOCHUBEI, G.N. KULIPANOV, N.A. MEZENTSEV, V.F. PINDIURIN, A.N. SKRINSKY and V.M. KHOREV
Institute of Nuclear Physics, 630090, Novosibirsk, USSR

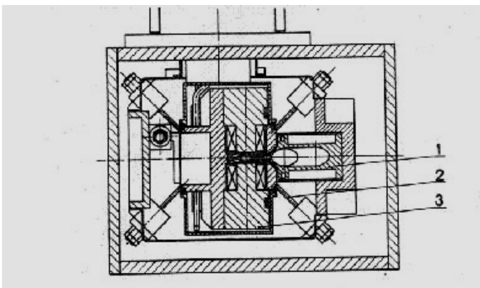

Cross section of the magnet with vacuum chamber

The wiggler cryostat was built in the traditional scheme of those times with use of liquid nitrogen and liquid helium with a consumption of approximately 4 l/hr. Main benefit of the wiggler installation on VEPP-3 storage ring was a 200 times increase of the photon flux in the photon energy range 15–20 keV.

Pole number	20
Pole gap, mm	15
Period, mm	90
Magnetic field amplitude, T	3.5
Vertical beam aperture, mm	7.8

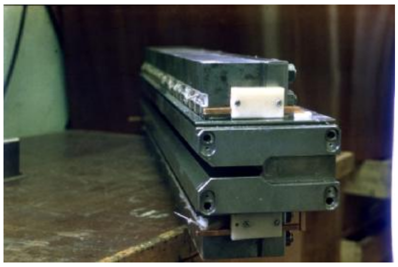

Photo of the wiggler magnet

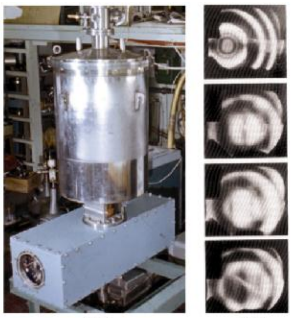

(A) (B)

A) The wiggler cryostat with magnet
B)Undulator radiation from the wiggler

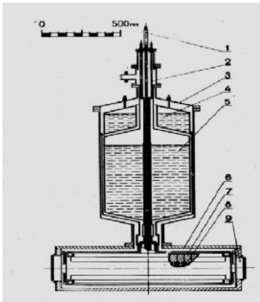

Sketch of the wiggler cryostat

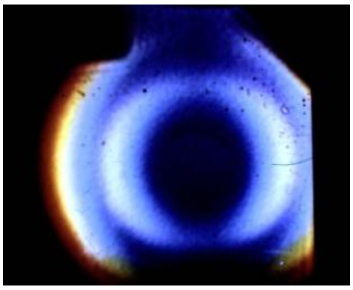

First superconducting undulator, ACO, Orsay, France

Tome 41 N° 23 1er DÉCEMBRE 1980

LE JOURNAL DE PHYSIQUE-LETTRES

J. Physique — LETTRES 41 (1980) L-547 - L-550 1er DÉCEMBRE 1980, PAGE L-547

Classification
Physics Abstracts
41.70 — 42.72

First results of a superconducting undulator on the ACO storage ring (*) (**)

C. Bazin (1), M. Billardon (2), D. Deacon (3) (5), Y. Farge, J. M. Ortega (2), J. Pérot (4), Y. Petroff and M. Velghe (5)

LURE, Bât. 209 C, Université de Paris-Sud, 91405 Orsay, France.

Abstract. A superconducting undulator has been fixed on the ACO storage ring. It has been observed that the electron beam is stable in the small gap of the vacuum chamber and unperturbed by the magnetic field of the undulator. Light emission has been observed at 140 and 240 MeV in the visible and ultra-violet. First results indicate that its geometrical as well as spectral distribution agree with theoretical predictions; small disagreements very probably arise from the fact that the electrons are not travelling exactly on the axis of the undulator.

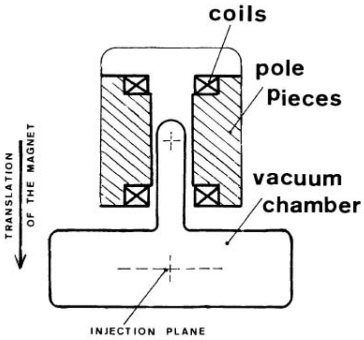

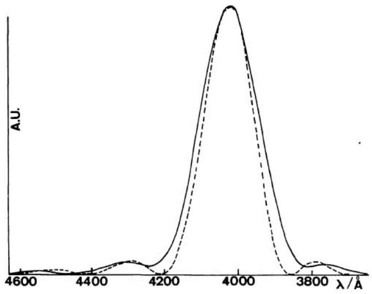

Fig. 4. — Spectral distribution of the emitted light (E = 150 MeV, K = 1.2) through a very small pinhole in the horizontal plane. Experiment : full lines; Theory : dashed lines.

Period	40 mm
Number of periods	23
Effective length	0.96 m
Maximum field Bo	0.45 T (K = 1.68).

Superconducting materials

Main properties of SC materials

The greatest interest from the point of view of creation of superconducting magnets represents such properties of superconductors, as critical temperature T_c, density of current J_c and field B_c. These parameters define position of critical surface in space with coordinates T, J and B and, hence, limiting characteristics of a magnet. Therefore it is desirable, that the specified critical parameters had higher values.

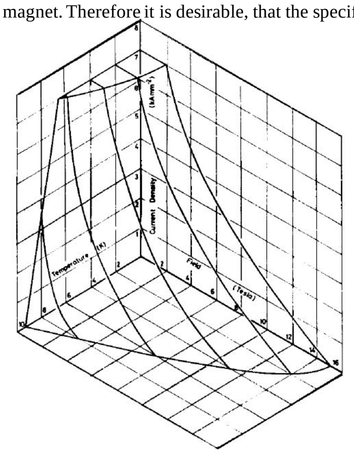

The critical surface of niobium titanium: superconductivity prevails everywhere below the surface and normal resistivity everywhere above it.

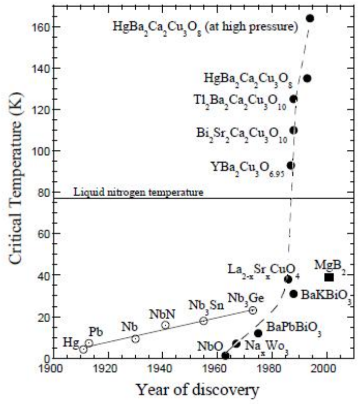

History of critical temperature of SC materials

B-T (critical field-critical temperature) and B-J (critical field – critical current) diagrams are shown in the figures below for best low temperature superconductors. Most of them exceed superconductors NbTi and Nb_3Sn by maximal magnetic field. However they, as a rule, essentially are more complex in manufacturing, and only two materials V_3Ga and Nb_3Al are possible to receive in the comprehensible form and the sufficient length for winding.

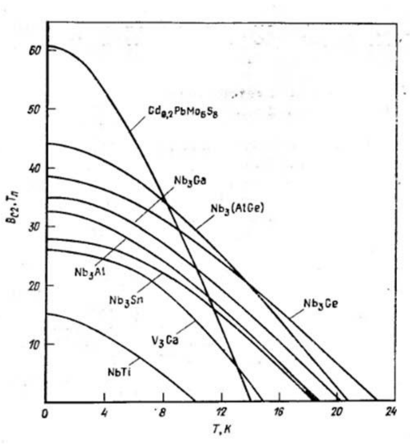

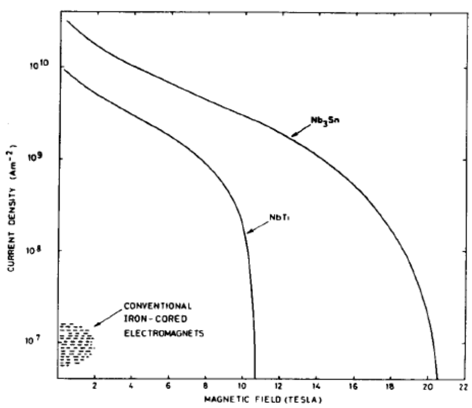

B-T critical curves of most popular SC materials for current in superconductors J=0A

B-J diagrame of Nb_3Sn and NbTi superconductors for 4.2K temperature

Nb-Ti/Cu SC wire

NbTi/Cu superconductor began one of the first to be used as a material suitable for magnet manufacturing. Owing to reliability and simplicity of windings manufacturing it still is the basic superconducting material for various magnets with field up to 8T.

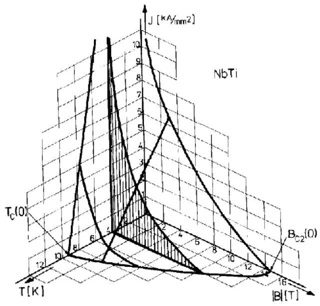

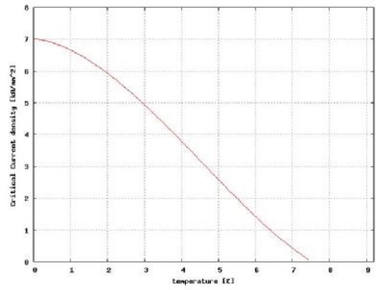

$$B_{C2}(T) = B_{C20}\left[1-\left(\frac{T}{T_{C0}}\right)^{1.7}\right]$$ Bottura's formula

B_{C2} ~ 14.5 Tesla at T=0K, T_{C0} ~9.2K at B=0T.

NbTi/Cu wire cross section

$$\frac{J_C(B,T)}{J_{Cref}} = \frac{C_0}{B}\left[\frac{B}{B_{C2}(T)}\right]^{\alpha}\left[1-\frac{B}{B_{C2}(T)}\right]^{\beta}\left[1-\left(\frac{T}{T_{C0}}\right)^{1.7}\right]^{\gamma}$$

C_0, α, β и γ – empirical parameters
Typical values: C_0=30T, α=0.6, β=1 и γ=2

Nb-Ti/Cu SC wire

There are two basic processes for Nb-Ti/Cu which are used for manufacturing of windings:

•Wet winding – epoxy coating is used during winding with special fillers for alignment of contraction coefficients between superconducting wire and epoxy coating, for increasing of heat capacity (Al_2O_3, Gd_2O_2S etc)

•Dry winding - vacuum impregnation or impregnation under pressure with hot (120^0C) hardening epoxy coating with corresponding fillers.

There is a technology of dry winding at which each coil layer is covering by the glass tape impregnated by silicon-organic varnish which hardens at low temperature, but at room temperature again becomes viscous.

Nb_3Sn/Cu SC wire

Magnet manufacturing with use of superconductors on base of Nb3Sn/Cu demands much more complex technology connected with baking out of a ready magnet at high temperature in vacuum or inert gas.

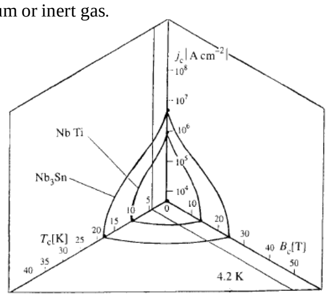

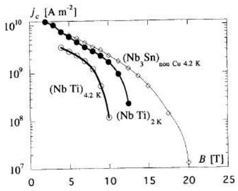

Comparison of NbTi and Nb_3Sn

Three main processes of fabricating Nb_3Sn wires:
- •Bronze process
- •Internal Sn process
- •Powder in tube (PIT) process

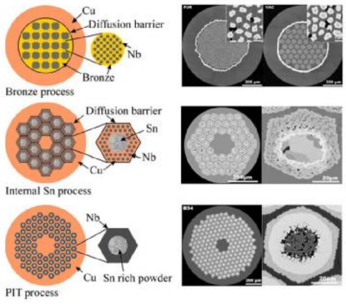

$$\frac{B_{C2}(T,e)}{B_{C20}(e)} = \left[1-\left(\frac{T}{T_{C0}(e)}\right)^2\right]\cdot\left\{1-0.31\cdot\left(\frac{T}{T_{C0}(e)}\right)^2\cdot\left[1-1.77\ln\left(\frac{T}{T_{C0}(e)}\right)\right]\right\}$$

$B_{C20}=30T$ critical field at T=0K

$T_{C0}=18K$ critical temperature at B=0T

$T_{C0}(e)=T_{C0m}\cdot\left(1-a\cdot|e|^{1.7}\right)^{\frac{1}{3}}$

a =900 for compressive deformation
a=1250 for tensile deformation

ε – deformation

Nb_3Sn/Cu SC wire

The Nb_3Sn wire will have superconducting properties at low temperature after baking out in vacuum or in inert gas at temperature 600-750^{0}C. But after this process the wire becomes very fragile as glass and there are technological restrictions at manufacturing windings with use such wire during bend.

Most technically comprehensible process of manufacturing of superconducting windings from Nb_3Sn is “Wind and react”. At this process the winding is made of a "crude" wire which has comprehensible properties for winding, and then the winding is baked out and as a result the wire possesses superconducting properties at low temperature.

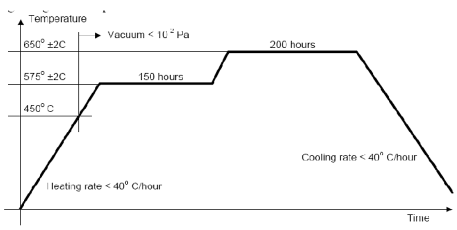

Process of baking out of Nb_3Sn/Cu coil

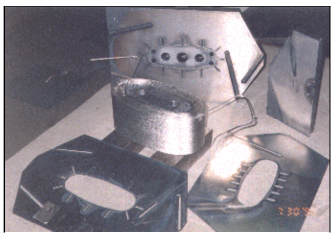

Nb_3Sn/Cu coil after baking out

High Temperature SuperConductors (HTSC)

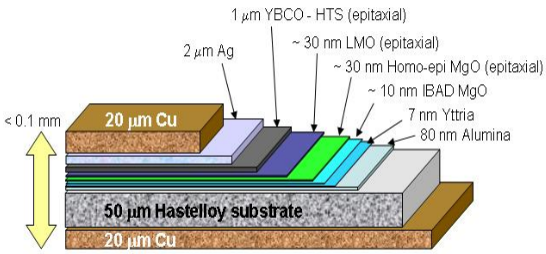

1G BSCCO-2223 Tape (AMSC)

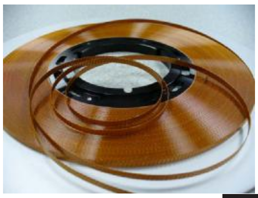

Bruker EHTS

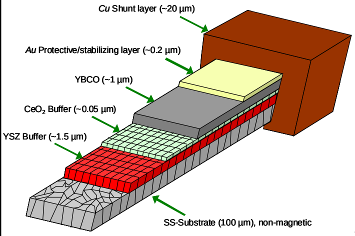

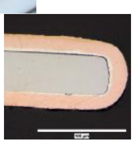

2G YBCO Wire (SuperPower, Inc.)

High Temperature Super Conductors (HTSC)

2G HTS has Excellent Performance Over a Wide Field and Temperature Range

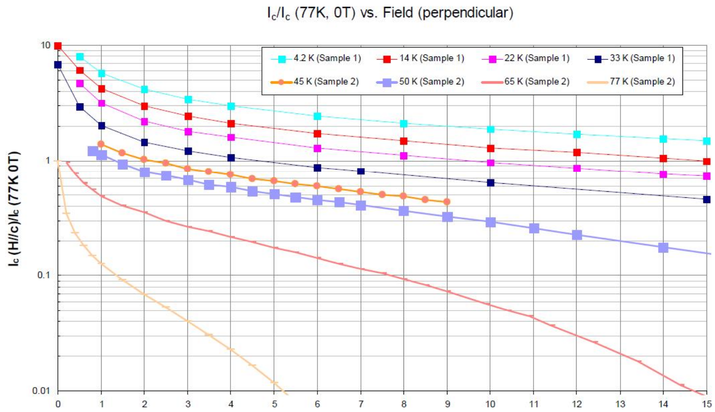

Critical current versus magnetic field for different orientation of tape and for various temperature.

SC coil design types for multipole wigglers and undulators

Peak Fields of Various ID Technologies

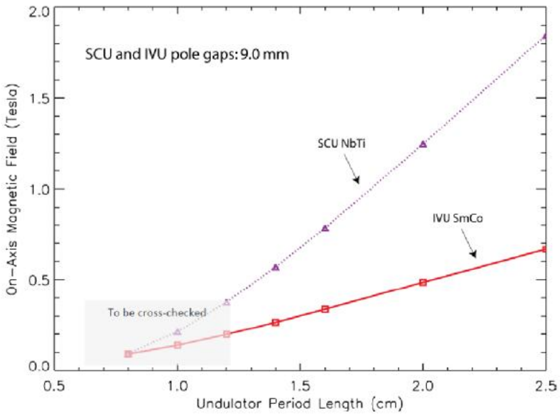

- Comparison of the magnetic fields in the undulator midplane for an in-vacuum SmCo undulator and a NbTi superconducting undulator versus the undulator period length at 9.0 mm pole gap.
- At 1.6 cm period length the fields are 0.34 Tesla (IVU) and 0.78 Tesla (SCU) – more than 2 times higher than that of the IVU.

Nb_3Sn wire may increase field by another 1.5 times

Planar coils:

•Horizontal racetrack coils

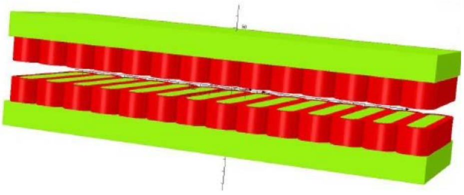

•Vertical racetrack coils

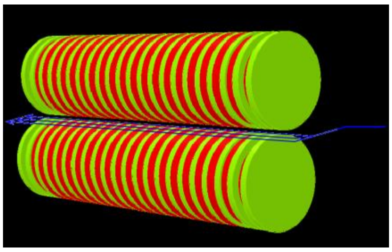

Comparison of horizontal and vertical racetrack coils

Horizontal racetrack	Vertical racetrack
Short SC wire is required	Long SC wire is required
Large number of splices for large number of poles.	Less number of splices.
Total SC wire length is minimal	Total SC wire length is 3-4 time more.
There is a possibility to make multi sections coils	There is no possibility to make multi section coils
The coils are stressed by bronze rods to compensate magnetic pressure in coils.	There is no possibility to stress coils by external compression
Minimal stored magnetic energy and inductance	Stored energy and inductance is more by 3 times
The coils have good thermo contacts with iron yoke after cooling down due to external compression	The thermo contacts became worth after cooling down. This is important disadvantage for indirect cooling magnets

Horizontal racetrack type (SC wigglers)

Budker Institute of Nuclear Physics

Magnet array of horizontal racetrack type poles (example of 30 mm period SC 2.1T wiggler)

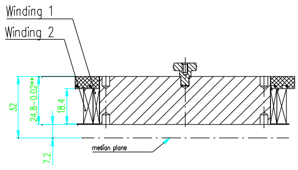

Drawing and photo of racetrack type poles (example of 2-sections coil of 48 mm period 4.2T wiggler

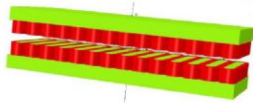

Horizontal racetrack coils assembly allows :
•to pre-stress all coils together for compensation of magnetic pressure
•to use 2 or more sections coils, which gives a possibility to obtain higher field for the same SC wire.

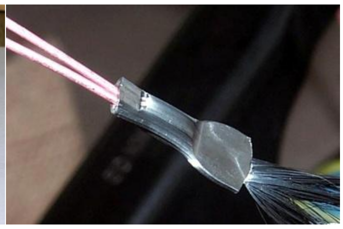

Cold welding method of wires connection gives resistance of the connection 10^{-10}-10^{-13} Ohm

Vertical racetrack coils (SC undulators)

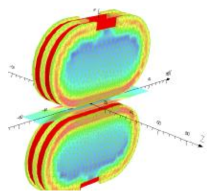

Argonne NATIONAL LABORATORY

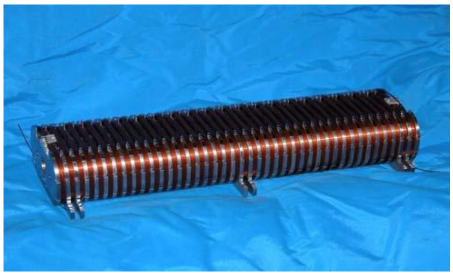

42 pole undulator APS prototype, period -16 mm

Magnetic structure layout

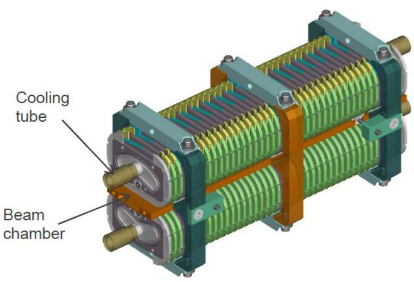

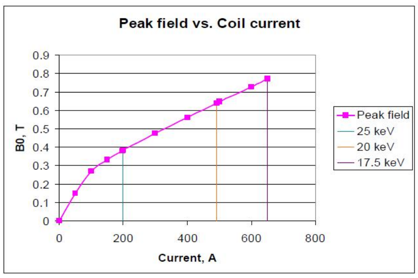

Vertical racetrack coils (SC undulators)

BABCOCK NOELL

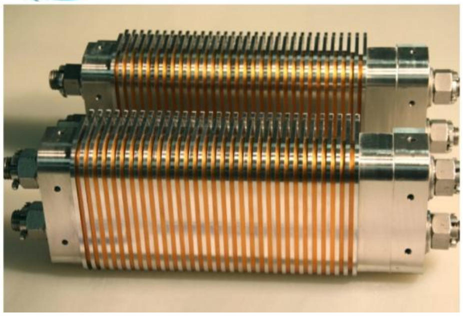

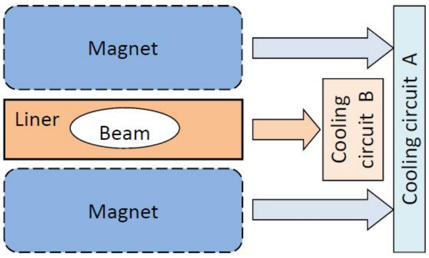

Under development in collaboration with ANKA

Period length, mm	15
Number of full periods -	100.5
Max field on axis with 8 mm magnetic gap, T	**0.77**
Max field in the coils,T	2.4
Minimum magnetic gap, mm	5.4
Operating magnetic gap, mm	8
Gap at beam injection, mm	16
K value at 5 mm gap -	>2
Design beam heat load, W	**4**

Vertical racetrack coils (SC undulators)

ACCEL

„Mock-up“ Prototype

- 10 Periods
- λ = 14 mm
- Gap = 5 mm
- B_{max} = 1,4 T @ 80% of sc-loadline
- K = 1,8
- End-pole correction

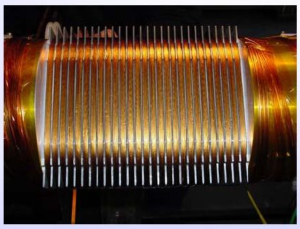

„Mock-up“ prototype; 10 periods

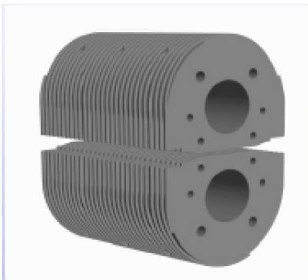

Prototype undulator (Mock-up)

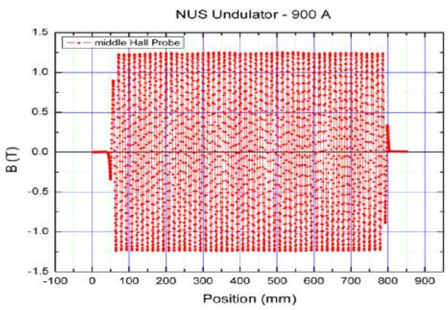

Vertical racetrack coils (SC undulators)

Jim Clarke
ASTeC, STFC Daresbury Laboratory

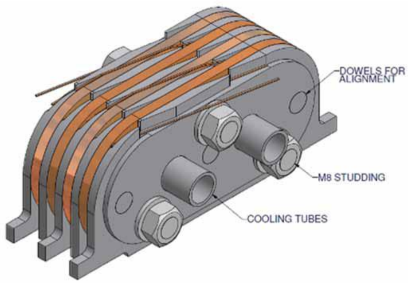

Magnetic length:	2 m
Period :	15 mm
Field on axis:	1.4 T
K	2.0
Beam stay clear:	5 mm (Vert.) x 50 mm (Horiz.)
rms phase error:	< 3 degrees
Trajectory straightness:	+/- 0.5 micron

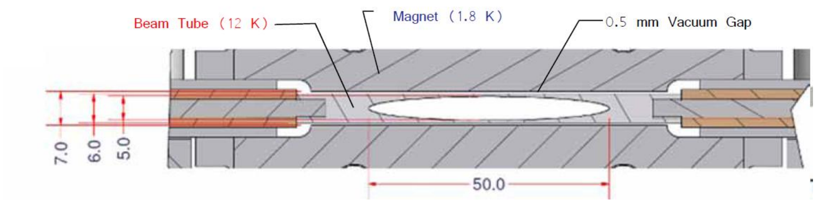

Vertical racetrack coils (SC wigglers)

LBNL
S. Prestemon, D. Dietderich,
S. Marks, R. Schlueter

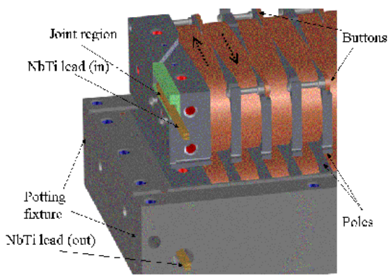

NbTi coils

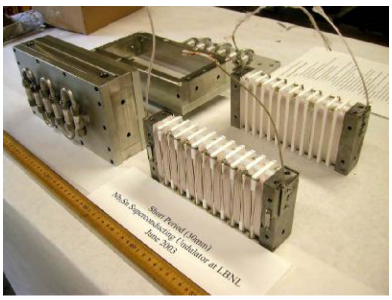

Nb $_3$Sn coils

Coil Geometry	
λ [mm]	30
p_w [mm]	4.8
c_w [mm]	10.2
c_h [mm]	5.4
y_h [mm]	28
Average turn length [mm]	21.9
Turns/layer	5
Number of layers	5
Conductor	
Strand diameter [mm]	0.48
Number of strands in cable	6
Cable width (bare) [mm]	1.75
Cable height (bare) [mm]	0.90
Insulation thickness [mm]	0.065
Cu:SC	1.08:1
RRR	21
Cabling packing factor	0.72
Overall SC fraction	0.24
J_c(5.9T, 4.2K) [A/mm^2]	6115
Anticipated performance (gap=10 mm)	
B_0 [T]	3.2
B_{max} [T]	5.9
I_{max} [A]	3200
E (stored energy/period) [J]	2000

Helical coils (SC helical Undulators)

Daresbury and Rutherford
Appleton Laboratories

SCU Helical constructed from NbTi (0.86T @ 11.5mm)

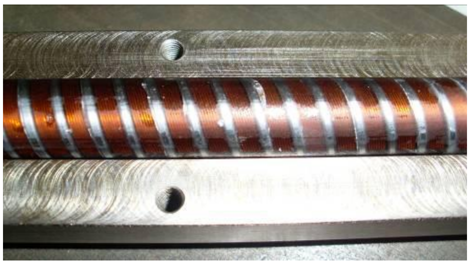

Nb3Sn short prototypes will be constructed soon (1.5T @ 11.5mm?)

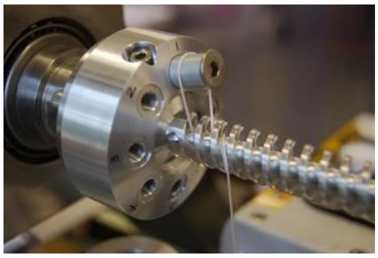

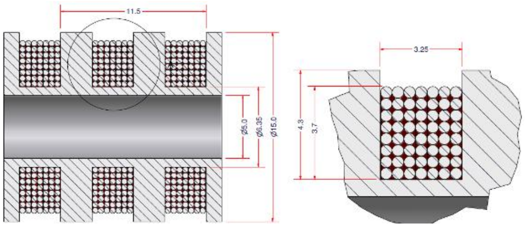

Double helical coils

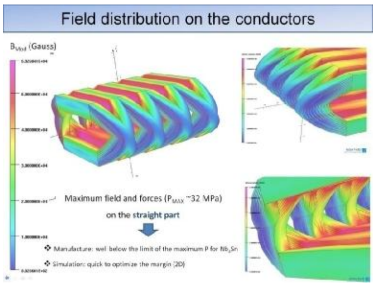

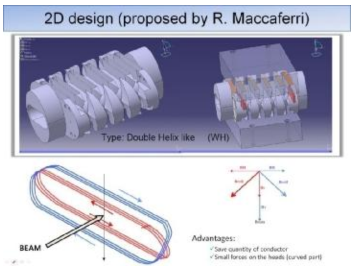

SC ID field calculations

1-section coils (example, SC wiggler)

Period, mm	30
Pole gap, mm	12.6
Pole number	119
Nominal field ,T	2.1

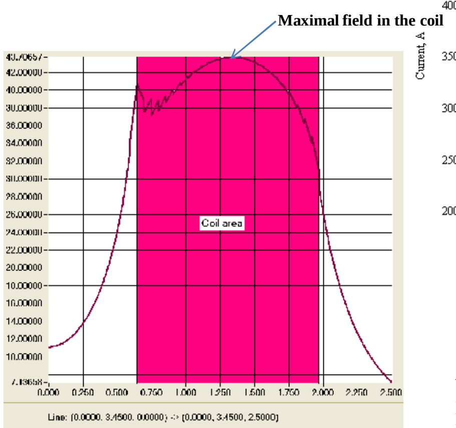

Magnetic field distribution at the inner radius of the coil along vertical coordinate (B, kGs; z, cm).

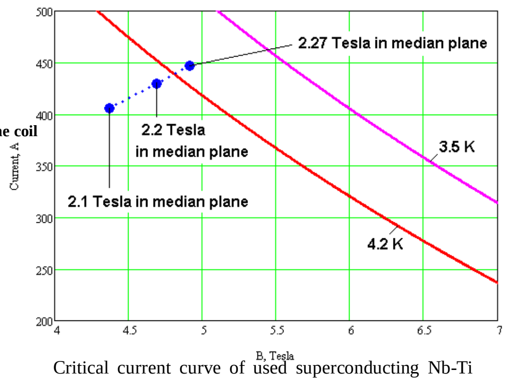

Critical current curve of used superconducting Nb-Ti and field-current critical points inside coil correspond to magnetic field in median plane. Temperature decreasing gives a possibility to increase field.

Wire parameters:

Wire diameter with/without insulation, mm	0.55/0.5
NbTi/Cu ration	1.4
Number of filaments	312
Diameter of filament, micron	37
Critical current at 7 Tesla, A	236

Comparison of one and two sections coils

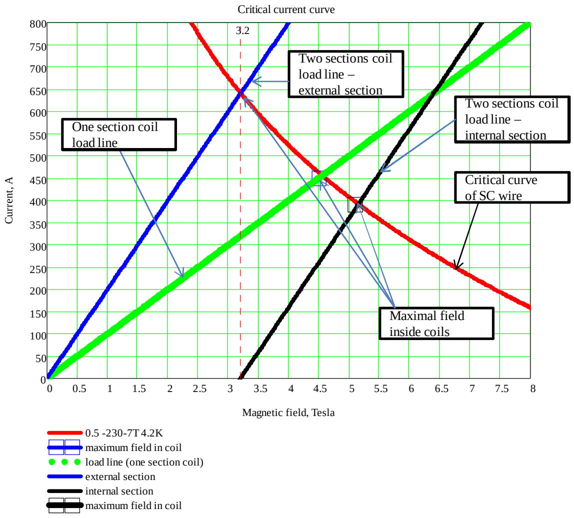

Figure shows a comparison of one and two section coils with identical layer numbers in the coils. The one-section coil reaches a critical current at 450A and field of 4.5T at internal layer. The two-section coil has different currents in sections which simultaneously reach critical values. The external section reaches a current of 649A and field of 3.2T at internal layer of the section. The internal section reaches a current of 380A and field of 5.2T at internal layer of the section. Due to splitting the coil into two sections with equal layer numbers and feeding section with different currents the field value increases by 15 % (5.2T and 4.5T) in comparison with an one-section coil. Maximal field may be increased by 30% in comparison with one section coil with use of independent current feedings of each coil layer. This approach requires a lot of independent power supplies and it is technical complication. Two-section coil is a reasonable compromise.

2-sections coils (example, SC wiggler)

Period, mm	48
Pole gap, mm	14.4
Pole number	49
Nominal field, T	4.1

Wire parameters:

Wire diameter with/without insulation, mm	**0.91/0.85**
NbTi/Cu ration	**1.4**
Number of filaments	**312**
Diameter of filament, micron	**37**
Critical current at 7 Tesla, A	**700**

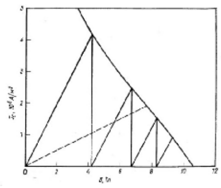

Load lines for 4-section magnet with separate feeding

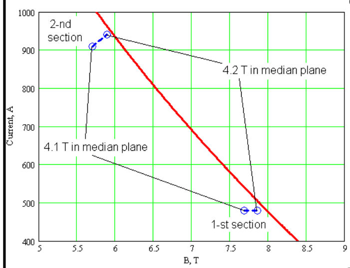

Critical current curve of used superconducting Nb-Ti wire (red line) and field-current critical points inside coil correspond to magnetic field in median plane

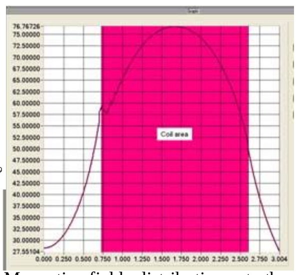

Magnetic field distribution at the inner radius of the coil 1-st section along vertical coordinate (B, kGs; z, cm).

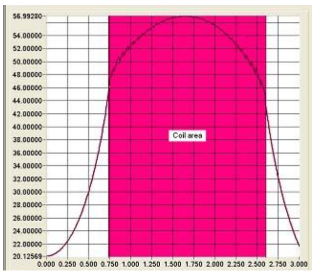

Magnetic field distribution at the inner radius of the coil 2-nd section along vertical coordinate (B, kGs; z, cm)

Two-sections coil gives up to 15% higher field for the same SC wire.

Magnetic field distribution in high field wigglers (Example of 7.5 T SC wiggler)

The magnetic flux inside of a pole in multipole wigglers and undulators is closing through the neighbor poles. In case of 2-dimensional field distribution (infinitely wide poles) the longitudinal field integral in median plane is automatically equal to zero. It follows from Maxwell's equations. At a high field in a wiggler iron cores are completely saturated and represent permanent magnets which give to the field some small contribution. This contribution may be increased with use some materials like Dy or Ho which are saturated at higher field. The maximal field inside the coils is on a wire layer which is nearest to an iron pole and approximately on half of height of the pole. This fact should be taken into account at field calculation as this part of the wire is most close to a critical curve on the diagram a field-current. External iron yoke is in use mainly as support system for poles and closes a stray field.

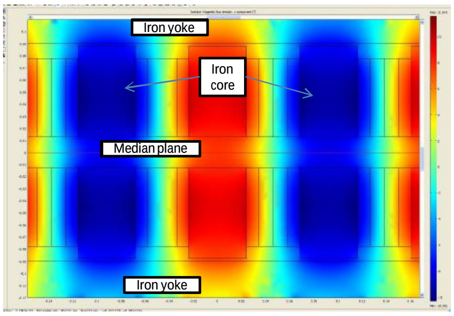

Vertical component of magnetic field distribution

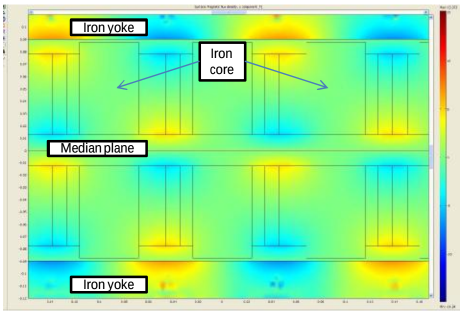

Horizontal component of magnetic field distribution

Lorentz forces in high field SC wigglers (Example of 7.5 T SC wiggler)

The forces acting on windings in horizontal direction, aspire to tear off the winding from the iron core. If there is no counteracting force a winding may move and as a result a heat will be extracted, temperature of a superconducting wire will rise up and the wire may transit to normal state (quench). Usually in such situations the further quench training of the magnet does not lead to field increasing. Presence of counteracting force may create a high pressure inside of windings (several hundreds bar) at which epoxy starts to crack with heat extraction. This also may be a reason of a quench. But here there is a hope, that quench training increase the field.

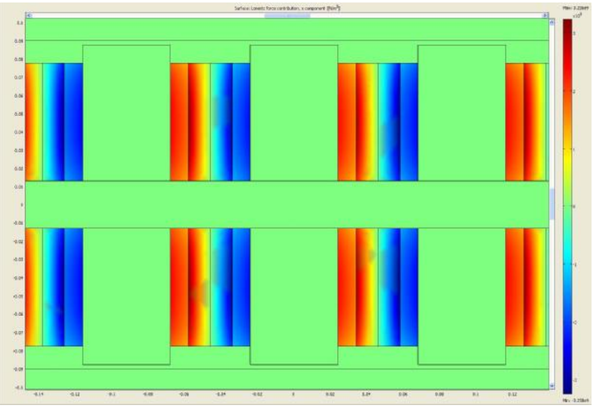

Distribution of horizontal component of Lorentz forces acting on windings

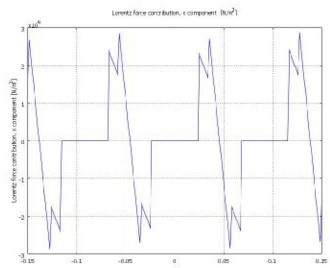

Horizontal component of Lorentz forces acting on windings along a horizontal line passing through middles of coils

Lorentz forces in high field SC wigglers (Example of 7.5 T SC wiggler)

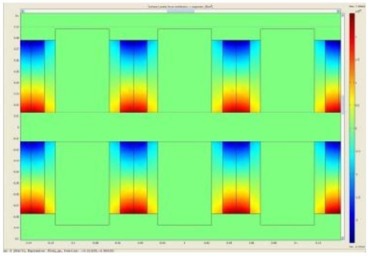

Lorentz forces (vertical component) acting on windings in vertical direction

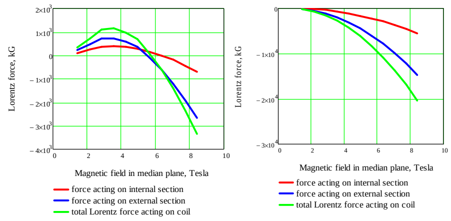

A B

Integral forces acting on coil sections versus field level . A) wiggler with iron yoke. B) wiggler without iron yoke.

The forces acting on windings, lead to their compression. Presence of iron yoke decrease integral force acting on windings.

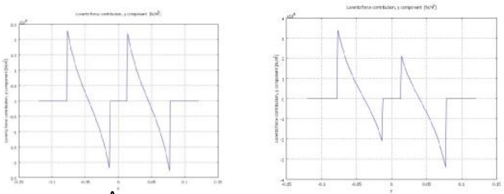

A B

Lorentz forces (vertical component) acting on windings in vertical direction along a vertical line passing through a coil mid. A)- wiggler with iron yoke, B)- wiggler without iron yoke

Main parameters of multipole SC ID

Main parameters of a superconducting multipole ID are:

λ_0- period,

B_0- magnetic field in median plane,

g- pole gap.

These parameters are linked by means of the formula:

$$B_0 = \frac{B_p}{\cosh\left(p\frac{g}{l_0}\right)} \approx B_p e^{-p\frac{g}{l_0}}$$

Bp - parameter is defined by magnet design and used superconducting materials.

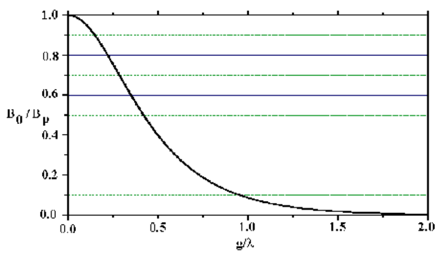

Ratio B_0/B_p versus g/l_0

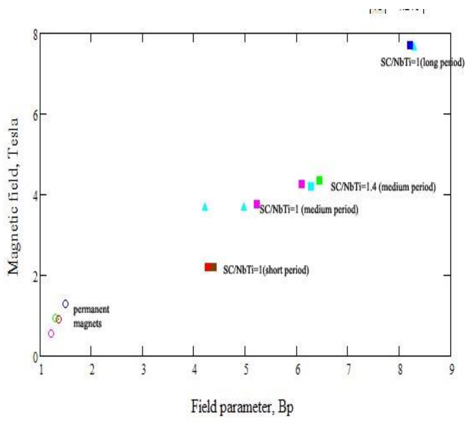

Correlation of Bp parameter with magnetic field for various SC wires

Transition of superconductor to normal state. (Quench)

Normal zone propagation

Quench is transition of a magnet in normal state occurs at occurrence in its winding of zones with normal resistance. As the superconductor in a normal state possesses high specific electroresistance, at presence in the winding of the magnet with high density current the superconductor in these zones is warmed up to the temperatures considerably exceeding its critical temperature, and the sizes of normal zones are increasing with time. This irreversible process leads to transformation of all energy reserved in the magnet into heat.

The energy necessary for translation of a winding in a normal state is rather small owing to low thermal capacities of materials at low temperatures: typical values of a thermal capacity at temperature of liquid helium approximately in 1000 times less than at room temperature.
The reason of a quench in a winding can be jumps of magnetic flux at ramp field, movement of badly fixed superconducting wire, epoxy crack, bad electric contact in a junction of wires, external heat in-leak.

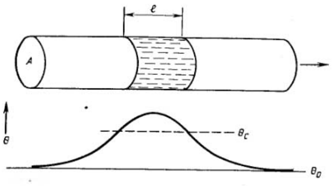

Appearance of a normal zone under action of local perturbation in a superconducting wire with current

$$l = \left[\frac{2k(q_c - q_0)}{rJ_c^{\,2}}\right]^{1/2}$$

J_c – critical current
l – minimal propagation zone (MPZ)
ρ- specific electroresistance
Θ_0, θ_c – temperatures

Quench initiation

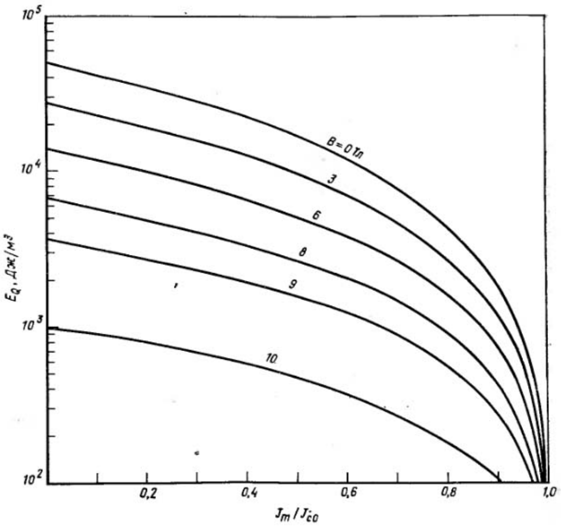

Threshold density of energy of volumetric perturbations for quench appearance in " a typical winding » at T=4.2K

Reasons:
- mechanical movement of SC wire
- crack of epoxy resin in coil
- heating of coil due to eddy current
- heating of coil due to bad electrical junction
- magnetic flux jump

Coil heating during quench

During propagation of normal zone inside magnet winding there is a non-uniform non-stationary temperature distribution changing within the limits of from 4.2K up to some maximal temperature θ_m in point the quench happened.

Thermal balance for normal zone:

$$J^2(t)\, r(q)\, dt = gC(q)\, dq$$

C- specific heat capacity,
γ – average winding density

$$\int_0^\infty J^2(t)dt = J_0^{\,2} t_d = \int_{q_0}^{q_m} \frac{gC(q)}{r(q)}\, dq = U(q_m)$$

Universal function U (θ_m) depends only on physical properties of the materials used in a winding, and allows to define the maximal temperature on initial current density in the winding and to characteristic time $\boldsymbol{t_d}$ attenuations of the current.

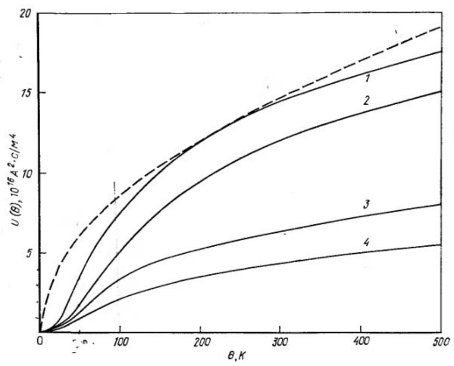

Function U(θ) for various conductors and typical magnet windings of small sizes.
1- copper RRR=150, 2-copper RRR=30, 3-aluminium ρ_0=5*10-11 Ohm*m, 4- winding (23 % NbTi, 47%Cu, 30 % epoxy.

Normal zone propagation velocity

$$v = \frac{J}{gC}\left(\frac{rk}{q_s - q_0}\right)^{1/2} = \frac{J}{gC}\left(\frac{L_0 q_s}{q_s - q_0}\right)^{1/2}$$

$L_0 = 2.45 \cdot 10^{-8}$ W*Ohm/K^2 – Lorentz constant

$$\frac{k}{s} = L_0 T \quad \text{Wiedemann-Franz-Lorentz law}$$

Useful relation between κ and *RRR* for copper

$$k \approx \left(\frac{RRR}{76}\right) \cdot T \quad \text{W/cm/K} \qquad (RRR = \sigma_{4.2K}/\sigma_{300K})$$

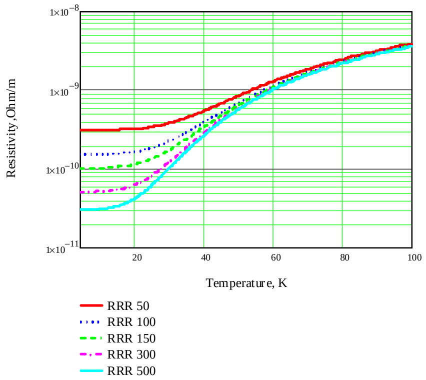

Copper electrical resistivity

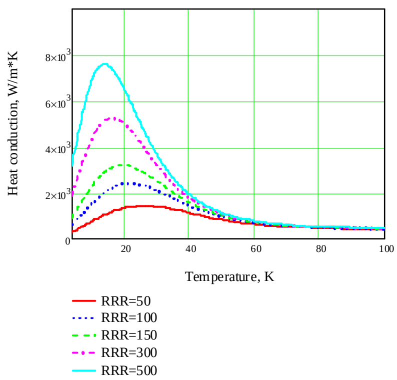

Copper heat conduction

Quench detection and quench protection

Quench detection

The high potential develops inside of a winding where exists resistive voltage component directed towards to inductive. The small voltage difference between feeding wires is caused by small internal resistance of power supply which is usually automatically disconnected at quench. But even if it will not occur, the voltage on the power supply is only some volt in comparison with hundreds and, probably, thousand volt in a normal zone. Therefore the voltage of the power supply can be neglected, but it should be disconnected quickly whenever possible to not admit a long heating winding inside a cryostat.

$$V_Q(t) = I(t)\cdot R_Q(t) + L_Q \cdot \frac{dI(t)}{dt}$$

$$I(t)\cdot R_Q(t) + L\cdot \frac{dI(t)}{dt} = 0$$

$$V_Q(t) = I(t)\cdot R_Q(t)\cdot\left(1-\frac{L_Q}{L}\right)$$

L – total inductance of a magnet,
L_Q- effective inductance of quenched magnet part.

Resistance of normal zone $R_Q(t)$ and its effective inductance L_Q grow with time, and current $I(t)$ is damping. Voltage V_Q in normal zone all over again grows up to the maximal value, and then decreases.

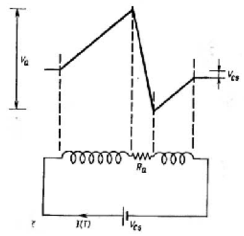

Electric potential distribution in a winding during quench

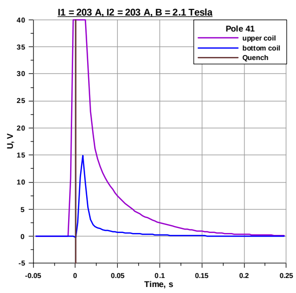

Time dependence of taps voltage of one section quenched coil

Quench detection

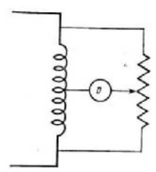

Bridge scheme of quench detecting

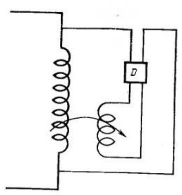

The scheme of quench detecting by means of a compensating winding

On bridge scheme the potentiometer is set in position at which gauge D does not react to current change in a magnet *dI/dT*. It is supposed, that gauge D registers voltage difference between top and bottom magnet sections caused by occurrence of a normal zone in a winding.

Compensating winding scheme is a registrator of transformer type in which the secondary winding is set on one of current leads and registers a signal *dI/dT* in magnet circuit. This signal amplifies, and then by the electronic detector is subtracted from the voltage of certain part of the winding.

Quench protection

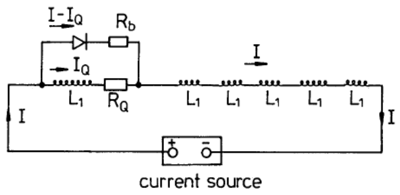

Passive quench protection scheme

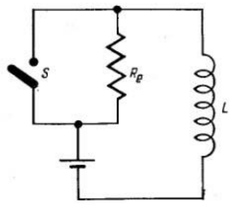

Active quench protection scheme

$$I = I_0 e^{-R_e T/L} = I_0 e^{-T/T_e}$$

$$\int_0^\infty J^2 dT = \frac{L I_0^2}{2A^2 R_e} = \frac{I_0^2 T_e}{2A^2} = U(q_m)$$

Cold Si diods are used as passive quench protection system in combination with dump resistor R_b. The cold Si diod is closed in both directions for voltage less than several volts. At higher volt the diod becomes normal diod. This property of the diod gives a possibility to ramp up and down field in a magnet without current branch, but if quench happened the diod opening and current flows through dump resistor.

Active quench protection scheme a magnet with inductance *L,* consists of external resistance *Rg* and switch *S*. During magnet feeding or operating conditions switch *S* is closed and the current practically does not flow through resistance *Rg*. As soon as quench detector will register the beginning of quench, switch *S* is disconnected and current flows through resistance *Rg*. If *Rg* is big enough in comparison with the resistance arising in the magnet the constant of time T_0 of circuits is defined by external resistance *Rg*.

Quench protection

Significant part of stored energy in a magnet may be extracted to external resistance as an element of magnet quench protection. It allows to reduce losses of liquid helium on evaporation at a quench and, besides to eliminate the usual danger connected with occurrence is excessive a high pressure inside cryostat as a result of boiling liquid helium. However reliability of such active method of protection entirely depends on non-failure operation of systems of registration and the breaker of a current. Therefore in many cases preference give passive ways of protection without application of any mechanical devices.

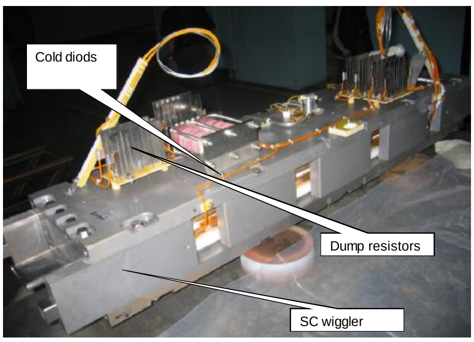

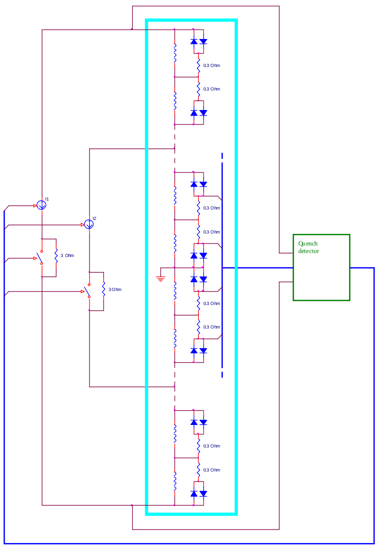

The electric scheme of protection of the partitioned superconducting magnet with use of "cold" diodes and external resistors

Quench training effect

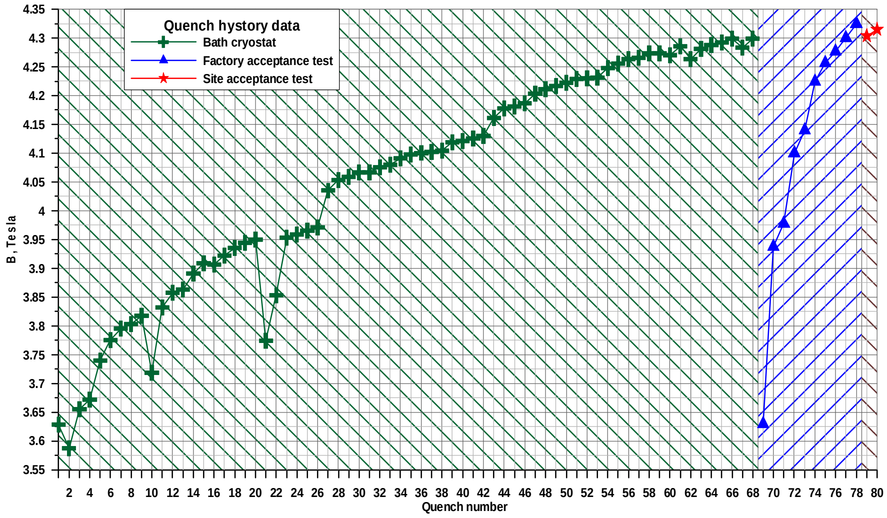

Example of SC wiggler for DLS training effect

Influence of SC ID field on beam dynamics

Field integrals

SC multipole wigglers and undulators represents sign-variable magnetic structure with many poles and with magnetic field defined by critical curve of a SC wire. Generally these devices are symmetrical or asymmetrical relative a mid point of magnetic structure. Main requirement for field feature is equality of first and second field integrals to zero. To provide this requirement two power supplies are used for feeding main and side coils.

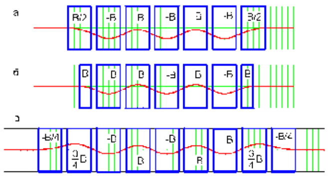

End poles are using for compensation of field integrals. Odd number of pole

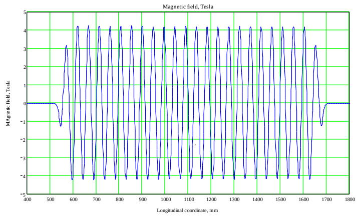

Field distribution in SC 4.2T wiggler with odd pole number

Field integrals along ID magnet

$$f = \frac{1}{Br}\int_{-L/2}^{L/2} B_z(s)ds = \frac{1}{Br}\int_{0}^{L/2} B_z(s)ds + \frac{1}{Br}\int_{0}^{L/2} B_z(-s)ds$$

First field integral (angle deviation of beam orbit inside ID with $B\rho$ beam rigidity). $B_z(s)$ – vertical component of ID magnetic field, s- longitudinal coordinate, L> ID length.
If $B_z(-s)= -B_z(s)$ –asymmetric system $\phi=0$
For symmetrical system $B_z(-s)= B_z(s)$ to provide $\phi=0$ currents in side poles should be adjusted.

The second field integral (orbit distortion inside L-interval:

$$d = \int_{-L/2}^{L/2} ds' \int_{-L/2}^{s'} \frac{B_z(s'')}{Br} ds'' = f \cdot L - \int_{0}^{L/2} \frac{s \cdot B_z(s)}{Br} ds + \int_{0}^{L/2} \frac{s \cdot B_z(-s)}{Br} ds$$

If $B_z(-s)= -B_z(s)$ asymmetric system and $\phi=0$, $d = -2\int_{0}^{L/2} \frac{s \cdot B_z(s)ds}{Br}$ is twice more than the orbit distortion at the ID mid point.

For cases a) and б) in the figure the integral is not zero but for symmetrical case $B_z(-s)= B_z(s)$ the integral is zero.
For case в) for both cases the integral may be set to zero using two power supplies.

Orbit inside ID

First field integral

$$x_0'(s) = \frac{1}{Br}\int_{-L/2}^{s} ds' B_z(s')$$

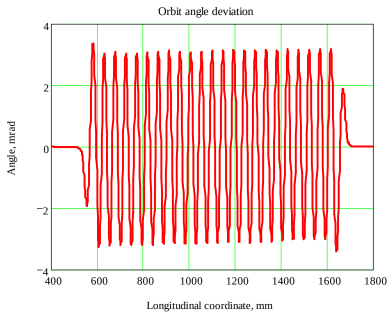

Angle orbit deviation inside 49-pole wiggler at field setting 4.2 Tesla, E=3 GeV

Second field integral

$$x_0(s) = \frac{1}{Br}\int_{-L/2}^{s} ds' \int_{-L/2}^{s'} ds'' B_z(s'')$$

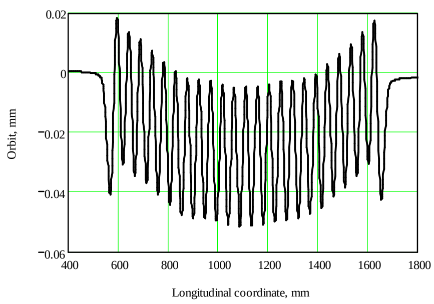

Orbit distortion inside 49-pole wiggler at field setting 4.2 Tesla, E=3 GeV

Phase space of electron orbit and photon beam

Electron beam orbit phase space

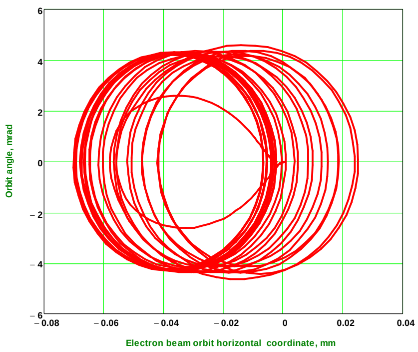

Photon beam phase space reduced to the wiggler center

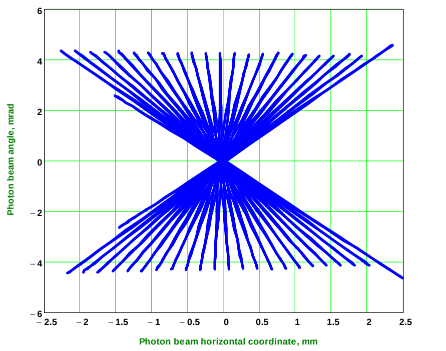

Focusing property of SC ID

$$x'' + K_x \cdot x = 0$$
$$z'' + K_z \cdot z = 0$$

Betatron motion equations

Local and integral focusing rigidity

$$K_x = \frac{B_z^2}{(B\rho)^2} + \frac{1}{B\rho}\left(x' \frac{\partial B_z}{\partial s} - \frac{\partial B_z}{\partial x}\right)$$

$$K_z = -\frac{1}{B\rho}\left(x' \frac{\partial B_z}{\partial s} - \frac{\partial B_z}{\partial x}\right)$$

$$\int_{-L/2}^{L/2} K_x ds = -\frac{\partial}{\partial x} \int_{-L/2}^{L/2} \frac{B_z ds}{B\rho}$$

$$\int_{-L/2}^{L/2} K_z ds = \int_{-L/2}^{L/2} \frac{B_z^2}{B\rho^2} ds - \int_{-L/2}^{L/2} K_x ds$$

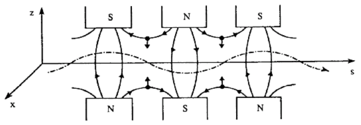

Vertical and horizontal tune shifts versus magnetic field, E = 1.9 GeV

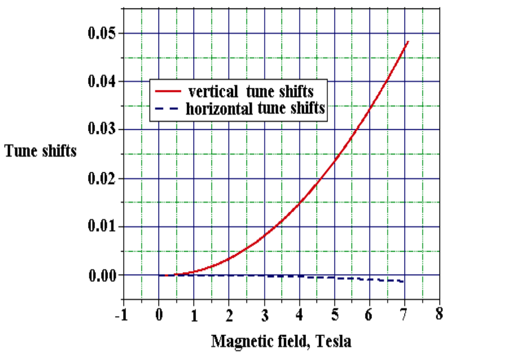

Vertical and horizontal betatron tune shifts for BESSY SC 7 T WLS versus magnetic field level.

Beating beta-functions

$$\frac{\Delta b_{x,z}}{b_{x,z}} = -\frac{K_{x,z} L b_{x,z}}{2\sin(m_{x,z})}\left(1-\frac{L^2}{12 b_{x,z}^{\;2}}\right)$$

Betatron ***β***-functions beating

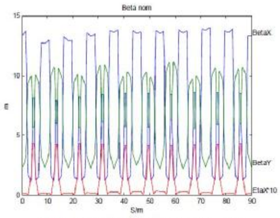

Machine functions from the calibrated model, no wiggler.

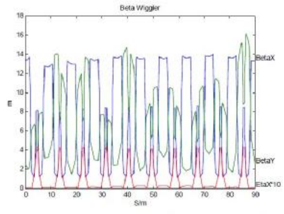

Machine functions from the calibrated model with wiggler.

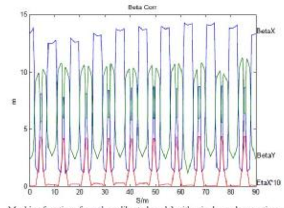

Machine functions from the calibrated model with wiggler and corrections.

The correction scheme used is based on reducing the vertical beta function in the wiggler.

A separate power supply increases the strengths of the adjacent vertical quadrupoles. The adjacent horizontal quadrupoles are also fitted with extra power supplies in order to compensate for the extra focusing in the vertical quadrupoles.

Since all of the changes so far have been increased focusing, an adjustment of the global tunes must be made by reducing the two quadrupole families.

These corrections were calculated using the calibrated model and then applied to the ring while the wiggler was at full current.

A new response matrix was measured and the measurment shows that this is an efficient method to correct machine optics.

E. Wallén

Effect of 3.5 Tesla SC wiggler installed on MAX-II ring,

Radiation (structural) integrals:

$$\Delta I_1 = \int_L \frac{(h_{x0} - x(s))B_z(s)}{Br} ds$$

a_x, b_x, g_x are Twiss parameters

$$\Delta I_2 = \int_L \frac{B_z^2(s)}{Br^2} ds$$

$$\Delta I_3 = \int_L \frac{|B_z(s)|^3}{Br^3} ds$$

$$\Delta I_4 = \int_L \left(\frac{B_z^3(s)\cdot}{Br^3} - \frac{2K_x}{Br}\right)(h_{x0} - x(s)) ds$$

$$\Delta I_5 = \int_L \frac{|B_z(s)|^3}{Br^3}\left(g_x(h_{x0}-x(s))^2 + 2a_x(h_{x0}-x(s))(h'_{x0}-x'(s)) + b_x(h'_{x0}-x'(s))^2\right) ds$$

$$\left(\frac{s'_E}{s_E}\right)^2 = \frac{1+\frac{\Delta I_3}{I_3^0}}{1+\frac{2\Delta I_2+\Delta I_4}{2I_2^0+I_4^0}} \approx 1+\frac{\Delta I_3}{I_3^0} - \frac{\Delta I_{24}}{I_2^0}$$

Energy spread change

$$\frac{e'_x}{e_x} = \frac{1+\frac{\Delta I_5}{I_5^0}}{1+\frac{\Delta I_2-\Delta I_4}{I_2^0-I_4^0}} \approx 1+\frac{\Delta I_5}{I_5^0} - \frac{\Delta I_2}{I_2^0}$$

Emittance change

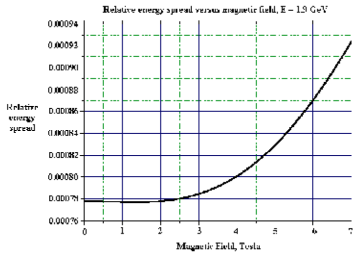

Energy spread in BESSY storage ring versus magnetic field level in SC 7 T WLS.

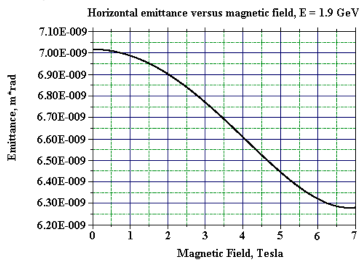

Horizontal emittance BESSY storage ring versus magnetic field level in SC 7 T WLS.

SC ID field expansion into multipole components

Magnetic field measurements of an ID are usually carrying out in Cartesian coordinates which will have designations χ, z, σ, thus the axis σ coincides with a longitudinal axis of an ID, χ and z are horizontal and vertical directions correspondingly. Planes z = 0, χ = 0, σ = 0 are corresponding planes of symmetry of WLS magnetic systems; therefore, the basic members of magnetic field expansion into multipole components in Cartesian coordinates, following K. Steffen (1965), may be written down in the forms:

$$B_z = a + \frac{b}{2}\cdot(c^2 - z^2) - \frac{a''}{2}\cdot z^2 + \frac{c}{24}\cdot(c^4 - 6c^2z^2 + z^4) - \frac{b''}{4}\cdot c^2z^2 + \frac{b''}{12}z^4 + \frac{a''''}{24}z^4 + \ldots$$

$$B_c = b\cdot cz + \frac{c}{6}\cdot(zc^3 - z^3c) - \frac{b''}{6}\cdot z^3c + \ldots$$

$$B_s = a'\cdot z + \frac{b'}{2}\cdot z(c^2 - \frac{z^2}{3}) - \frac{a'''}{6}\cdot z^3 + \ldots$$

The primes in formulas mean a derivative on longitudinal coordinate s. We shall designate $x_0(s), x_0'(s)$ as coordinate and angle of beam orbit deviation to a ID axis accordingly. In displaced on coordinate $x_0(s)$ and rotated on angle $x_0'(s)$ the basic field multipole components (field, gradient, and sextupole) may be expressed as:

$$B_z = a + \frac{b}{2}\cdot x_0^2 + \frac{c}{24}\cdot x_0^4 + \ldots$$

$$G = b\cdot x_0 + \frac{c}{6}\cdot x_0^3 - x_0'(a' + \frac{b'}{2}x_0^2 + \frac{c'}{24}x_0^4) + \ldots$$

$$S = b + \frac{c}{2}x_0^2 - 2b'x_0x_0' - \frac{c'}{3}x_0^3x_0' + a''x_0'^2 + \frac{b''}{2}x_0^2x_0'^2 + \ldots$$

If magnetic system is homogeneous enough so that orbit deviation $x_0(s)$ is much less than characteristic size of field decrease, the formulas may be simplified:

$$B_z = a + \frac{b}{2}\cdot x_0^2$$

$$G = b\cdot x_0 - x_0'a'$$

$$S = b - 2b'x_0x_0' + a''x_0'^2$$

SC ID field expansion into multipole components

Magnetic field of multipole ID with periodic magnetic field may be approximated by formulas:

$$B_z = B_0 \cos(k_0 s)\cos(k_x c)\cosh(k_z z)$$

$$B_c = -\frac{k_x}{k_z} B_0 \cos(k_0 s)\sin(k_x c)\sinh(k_z z)$$

$$B_s = -\frac{k_0}{k_z} B_0 \sin(k_0 s)\cos(k_x c)\sinh(k_z z)$$

Where $k_0 = 2p / l_0$, $k_x = 2p / l_x$, $k_z = 2p / l_z$; l_0, l_x, l_z are wiggler characteristics magnetic field periods in s, c, z-directions and $k_z^2 = k_x^2 + k_0^2$ are following from Maxwell equations

Field, gradient, and sextupole components in approximation $k_x x_0 << 1$, $x_0' << 1$ may be expressed as:

$$B_z(s) = B_0 \cos(k_0 s)(1 - \frac{1}{2} k_x^2 x_0^2(s) + \ldots)$$

$$G(s) = B_0 \left(\cos(k_0 s)(-k_x^2 x_0(s) + \ldots) + \sin(k_0 s)(x_0'(s) k_0 + \ldots)\right)$$

$$S(s) = B_0 \left(\cos(k_0 s)(-k_x^2 - k_0^2 x_0'(s)_0^2 + \ldots) + \sin(k_0 s)(-2k_x^2 k_0 x_0(s) x_0'(s) + \ldots)\right)$$

$$x_0'(s) \approx \frac{B_0}{k_0 B r} \sin(k_0 s)$$

$$x_0(s) \approx \frac{-B_0}{k_0^2 B r} \cos(k_0 s)$$

SC ID cryogenic systems

Bath cryostat systems

The basic cryostat function is maintenance of SC wiggler magnets at temperature of liquid helium of 4.2 K. The wiggler magnet is placed into a bath with liquid helium and all heat emission inside the magnet and heat in-leak outside lead to liquid helium evaporation process. The cryostat consists of external vacuum housing, 60 K and 20 K shield screens, liquid helium vessel with a SC multipole magnet inside, throat, vacuum chamber (beam duct) with copper liner inside, upper flange, filling tube, two 2-stage coolers with stage temperature 4.2 K/50 K, and two 2-stage cryocoolers with stages temperature 20 K/50 K for shield screen cooling.

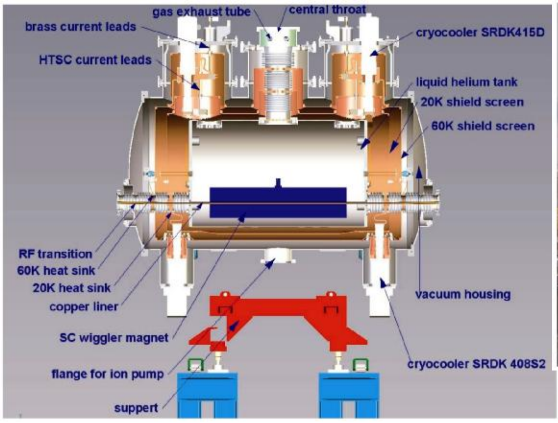

Pattern of a cryostat cross section.

Photo of SC wiggler installed on CLS storage ring.

Bath cryostat systems (shield screens)

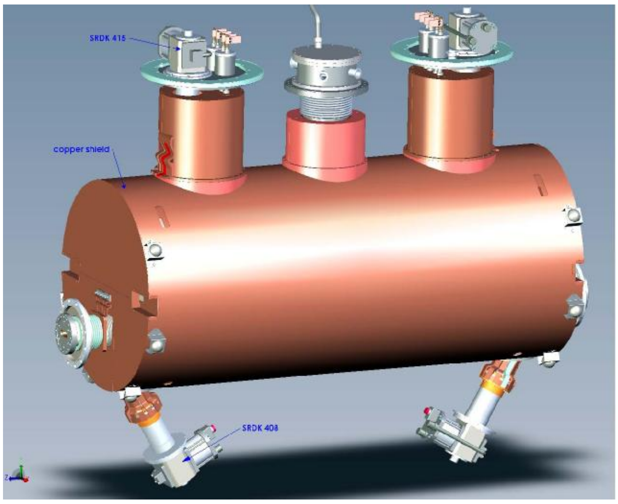

The inner liquid helium vessel is surrounded by two shield screens to reduce the irradiation heat flux from outside. The temperature on the outside shield screen is about 60 K, and on the inner one the temperature is about 20 K.

Shield screens are made of copper by thickness of 3 mm. The 60K and 20K copper screens are assembled to common block and inserted into the cryostat housing using special fiber glass balls. The 60 K screen is attached to all of four 60 K stages of the coolers by heat sinks. The 20 K stages of the both bottom coolers are connected to copper liner and to 20 K screen. The 4 K stages of top cryocoolers are attached to HTSC current leads and to liquid helium vessel. The external 60 K screen is covered by 30 layers of cryogenic superinsulation.

Bath cryostat systems (LHe tank)

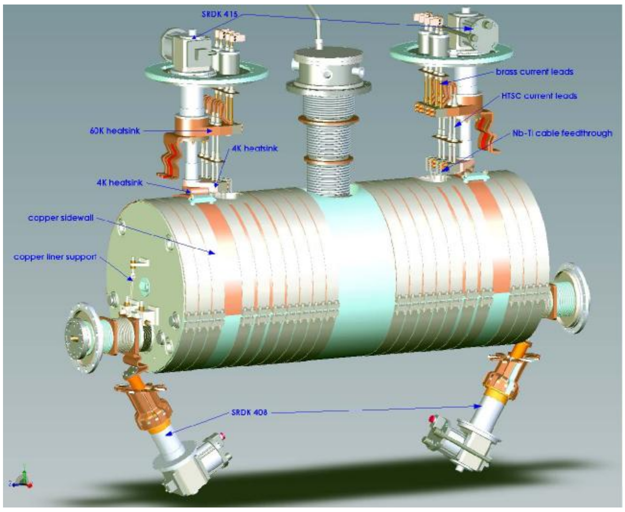

There is vacuum insulation between the helium vessel and external warm stainless steel vessel to reduce the residual gas heat flux. The helium vessel is suspended with four vertical and four horizontal kevlar straps connected to the external cryostat vessel. These straps pass throughout the both shield screens and attach to bolts on the external housing walls and are used for precise alignment of the vertical magnet position. Superconducting magnet is inserted into the liquid helium tank which is located inside of the shield screens and fixed on four vertical and four horizontal Kevlar suspension straps attached to the external housing. The helium vessel is a 316LN stainless steel barrel with the wall thickness of 6 mm. The axis of barrel is oriented horizontally.

Cryostat heat load budget

Main processes of heat load:

-heat conduction $$Q = \frac{-1}{\int_{x_1}^{x_2} \frac{dx}{A(x)}} \left[\int_{T_1}^{T_2} k(T)\,dT \right]$$

-radiation $$Q = e \cdot s \cdot A \cdot T^4$$

-image current of electron beam

	First 60K shield screen, Watt	Second 20K shield screen, Watt	LHe vessel 4.2K, Watt
Radiation	8	0.7	0.0001
Central throat bellows	5	0.9	0.03
Vacuum chamber bellows	8	0.7	0.02
Support system	0.5	0.01	0.01
Current leads heat conduction	70	0	0.5
Current leads Joule heat	60	0	0.2
Measuring wires	5	0.1	0.1
Liner	0	10	0.2
TOTAL	**156.5**	**12.41**	**1.0601**
Cooling machine capacity	**210**	**25**	**3**

1 W=1.4 liter/hour of Lhe at 4.2K, or ~2.6kJ=1liter of LHe

Cryocoolers capacity (example)

SRDK 415 D – W71D	
Refrigeration Capacity First Stage Second Stage	35W/45W @ 50 K (50/60Hz) 1.5 W @ 4.2 K Max. (50/60Hz)
Weight	18.5 kG

SRDK 408 S2 – W71D	
Refrigeration Capacity First Stage Second Stage	35W/40W @ 50 K (50/60Hz) 5.4/6.3 W @ 10K K Max. (50/60Hz)
Weight	18.5 kG

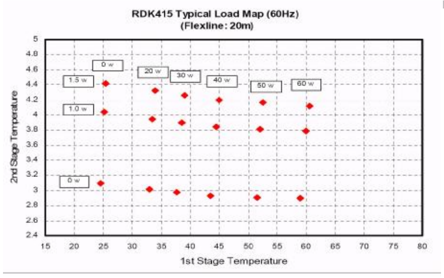

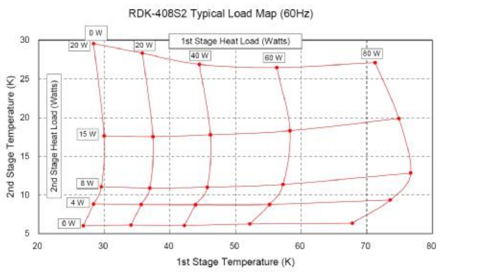

Beam vacuum chamber system

Insulating vacuum is separated from UH vacuum of a storage ring and keep at vacuum level $10^{-6} – 10^{-7}$Torr by 300l/s ion pump

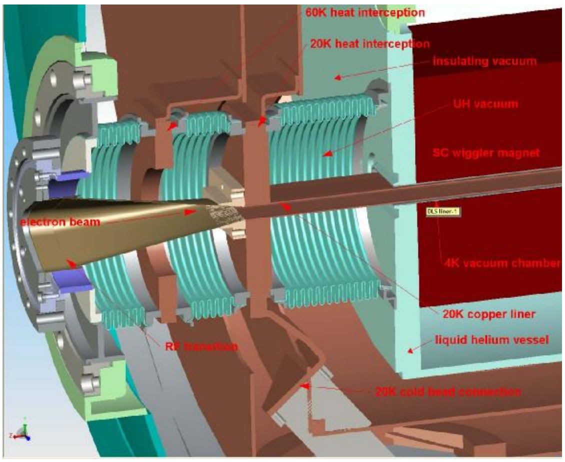

Liquid helium vessel with vacuum chamber fittings

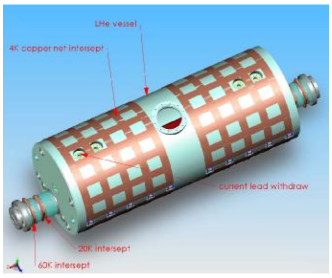

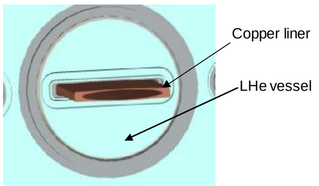

Protection of liquid helium vessel from electron beam heating (copper liner)

Beam heating effect:
- synchrotron radiation from upstream bending magnet
- image currents
- wake fields
- electron clouds

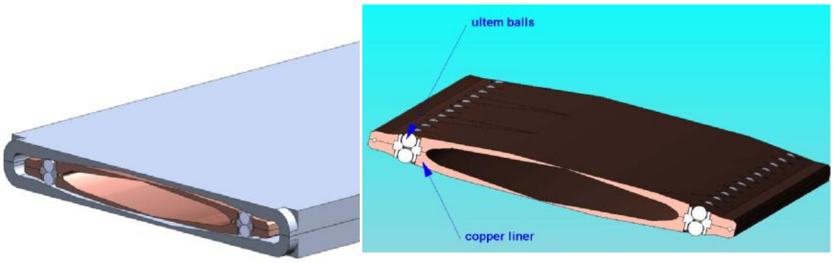

Pole gap and electron beam vertical aperture

As it was already mentioned above, the formula for multipole IDs forms a bond of key wiggler parameters: field, period, and pole gap. That strongly limits freedom of a choice. Low limit of beam vertical aperture of modern storage rings is about 6–7 mm by requirements of beam dynamics in storage rings.

In the bath cryostat design, it is supposed that inside of pole gap, a vacuum chamber and 20 K shield screen should be installed. The vacuum chamber is a part of liquid helium vessel and has temperature of 4.2 K. Shield screen with temperature 20 K (copper liner) absorbs heat which is raised by electron beam moving inside the copper liner (SR, heating by image currents, etc.).

Direct cooling magnet with liquid helium (magnet in bath cryostat)

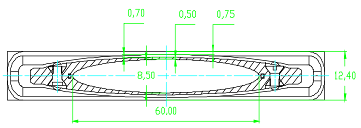

Pole gap= V aperture + 4 mm

Indirect cooling magnet
Magnet in insulating vacuum

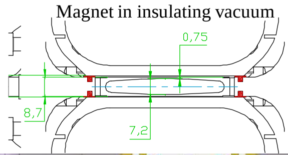

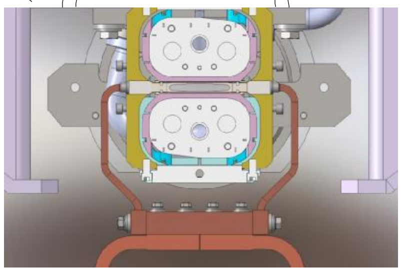

Pole gap = V aperture + 1.5 mm

Cryogenic System of indirect cooling of magnet

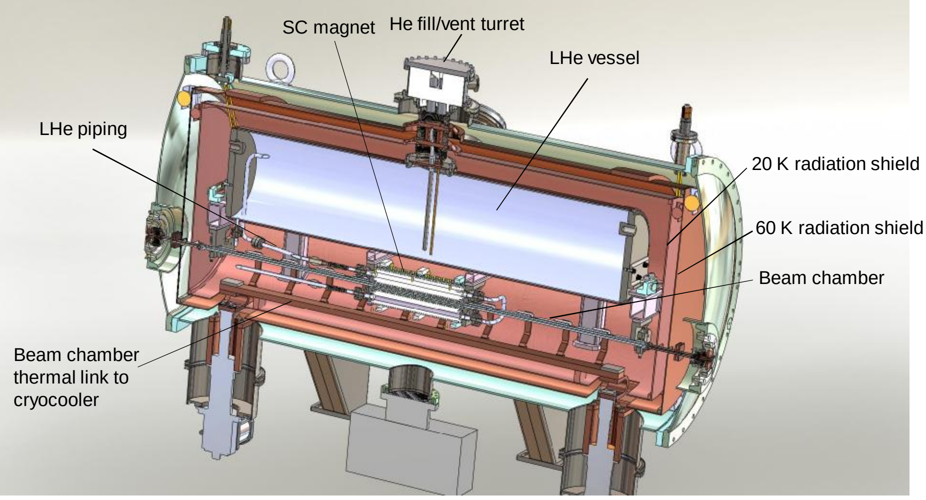

Example of cryostat with indirect cooling of undulator magnet in APS

Current feeding of SC ID

Electrical connections

Two power supply units are used to feed the central and side coils. Such connection gives a possibility to control the field integral to zero with required accuracy.

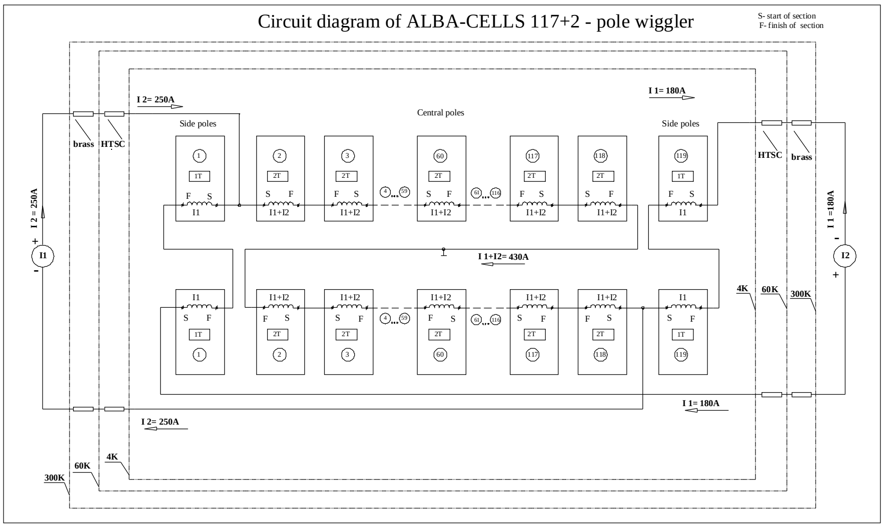

Normal conducting current leads

The primary goal of current leads design is minimizing heat in-leak into cryostat at set current in a magnet. This heat in-leak has two components: one is caused by current leads heat conductivity, and another — Joule heat. Therefore it is natural, that heat conductivity and current leads electroresistance should be minimal. However, according to law Wiedemann–Franz low these two metal properties are linked:

$$\frac{\kappa}{\sigma} = LT \quad L = \frac{\kappa}{\sigma T} = \frac{\pi^2}{3}\left(\frac{k_B}{e}\right)^2 = 2.44 \times 10^{-8}\,\mathrm{W\,\Omega\,K^{-2}}$$

This low is well enough correct for majority of metals and alloys. It means that the minimum heat in-leak into cryostat depends not on current leads material but on their form and dimensions.

The equation for temperature distribution along not cooled by gas current leads with a current is as follows:

$$\frac{d}{dx}\left[k(q)A\frac{dq}{dx}\right] + \frac{I^2 r(q)}{A} = 0$$

Not cooled by gas current are used as the first step combined тcurrent leads from normally spending metal in a range of temperatures 300K-70K. The second part of current leads consists of a warm superconductor in a range of temperatures 70K-4K.

For optimal current lead calculated for current I_0 made of pure copper the heat in-leak due to heat conduction is equal to $W/I_0=0.7*10^{-3}$ W/A if there is no current, but for electro- technical copper the heat in-leak is $W/I_0=0.4*10^{-3}$ W/A.

Than a current lead material (i.e. the it has smaller heat conductivity) is less pure, it is more suitable for current leads.

Combined normal and high temperature SC conducting current leads

Feeding current is passing through current lead which consists of normal conducting brass current lead and high temperature superconducting (HTSC) current lead. The current leads are grouped on two special current leads blocks together with cryocoolers. The top ends brass current leads are connected to power supplies at room temperature in an atmosphere. The brass current leads feedthrough into insulating vacuum volume and their bottom ends have thermal contact with first stage of cryocoolers for interception of heat in-leak at temperature 55-60K. In the point of heat interception the brass current leads are connecting HTSC current leads. The junction is supervised by the temperature probes as interlocks for HTSC current leads safety if the temperature of this current leads above 70K.

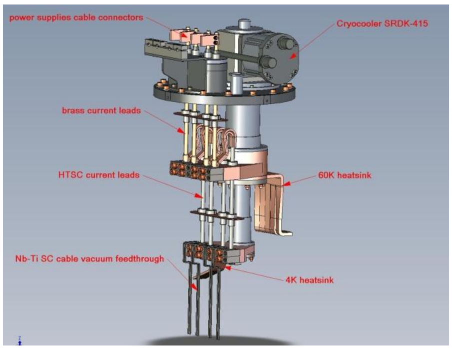

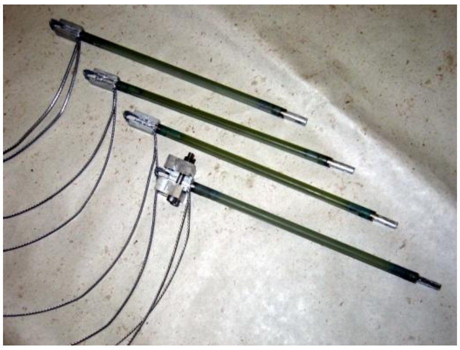

SC ID magnetic measurements systems

Hall probes measurements

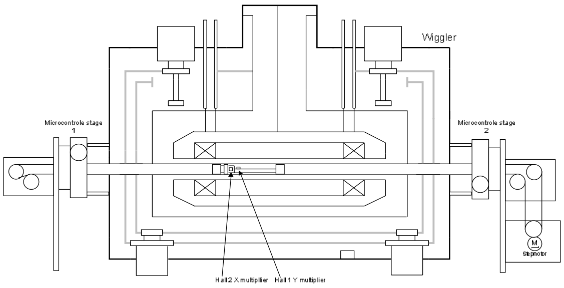

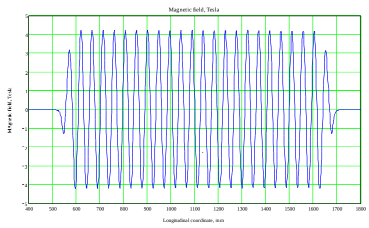

Longitudinal field distribution

Parameters:
- 2 Hall probes mutually perpendicular
- Temperaure probe
- Steps defined by step motor
- Ti-tube is warming up to room temperature by DC
- Ti-tube horizontal by microcontrol stage translation ± 20 mm
- Ti-tube vertical manual translation ±5 mm

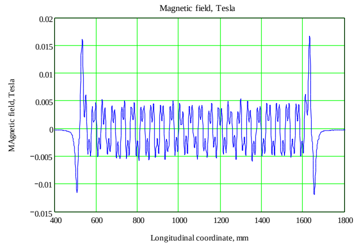

Field distribution at zero currents (after normal operation)

Field integrals measurements with stretched wire method

Main purposes:
- To make a table of currents (main and correctors) to provide field ramping up and down without orbit distortion
- To minimize field ramping time
- To estimate field multipole integrals at any field level

A method of strained wire with a current was used for field measurements and coil currents matching. The method is based on a very similar behavior of the wire with dc current in magnetic field and electrons moving along this magnetic field.

The wire strained by a force P was passed through the vacuum chamber of the wiggler. At the ends of the wiggler, the two Wire Position Probes (WPP) were installed to measure displacements of the wire during the experiment. The space resolution of WPPs is about 0.005 mm.

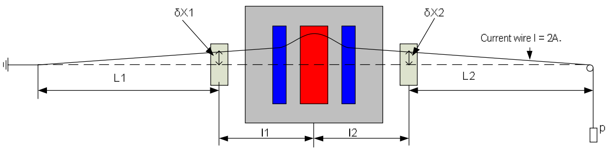

Parameters:
L1=L2~2-3 m
I~0.5-2 A
Wire- brass 0.3 mm diam.
WPM accuracy – 3-5 mkm
Tension force - ~ 10 N
1-st Field integral accuracy - ~$4*10^{-5}$ T*m
2-nd field integral accuracy- ~ 10^{-4} T*m^2

Motivation of the method

$\frac{d^2x}{ds^2} = \frac{B(s)}{Br}$ - beam orbit in magnetic field B(s), Br - beam rigidity

$E \cdot J \cdot \frac{d^4x}{ds^4} + T \cdot \frac{d^2x}{ds^2} = I \cdot B(s)$ - bending of stretched wire with current in magnetic field B(s)

$\frac{T}{I}$ - Rigidity of stretched wire with current

First term of equation for wire may be neglected for thin wire

$\frac{d^2x}{ds^2} = \frac{I}{T} \cdot B(s)$ The equations for beam and for wire are identical for $Br = \frac{T}{I}$

Beam orbit and wire bends are described by formulas (L-magnet field length) if initial angle and coordinate are equal to 0 at ±L/2:

$I_1(s) = \int_{-L/2}^{s} B_z(s')ds'$ $\quad \frac{dx(s)}{ds} = \frac{I_1(s)}{Br}$ angle deviation of beam orbit or wire at s-position

$I_2(s) = \int_{-L/2}^{s} ds' \int_{-L/2}^{s'} B_z(s'')ds''$ $\quad x(s) = \frac{I_2(s)}{Br}$ X-coordinate of beam orbit or wire at s-position

$da = \frac{I_1\left(\frac{L}{2}\right)}{Br}$ $\quad dx = \frac{I_2\left(\frac{L}{2}\right)}{Br}$ Angle and coordinate at L/2

$da = \frac{dx1}{L1} + \frac{dx2}{L2}$ Total angle deviation $I_{first} = I_1\left(\frac{L}{2}\right) = da * \frac{T}{I} = \frac{T}{I}\left(\frac{dx1}{L1} + \frac{dx2}{L2}\right)$

$dx = dx2 - dx1$ Orbit distortion at condition $da = 0$ $I_{second} = I_2\left(\frac{L}{2}\right) = dx \cdot \frac{T}{I} = \frac{T}{I}(dx2 - dx1)$

Scheme of measurements and data readout

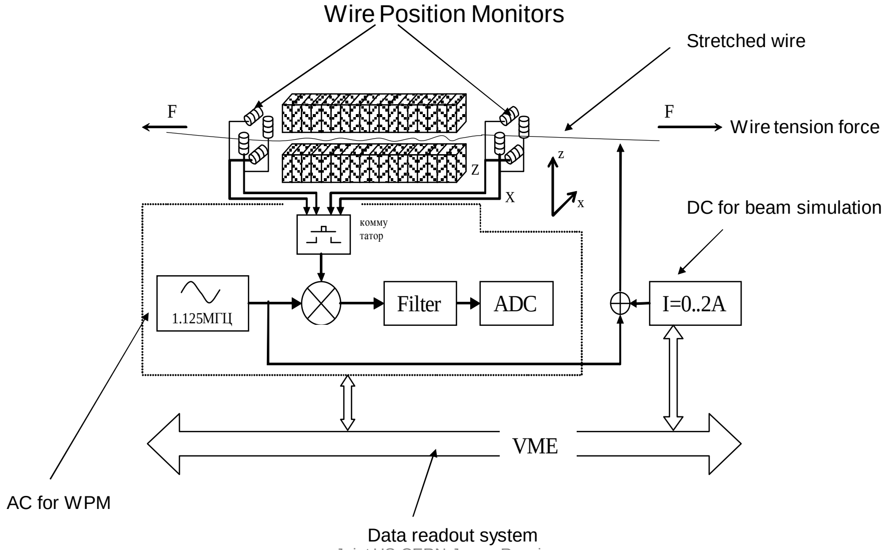

Results of measurements

Field ramping with zero field integrals using two power supplies

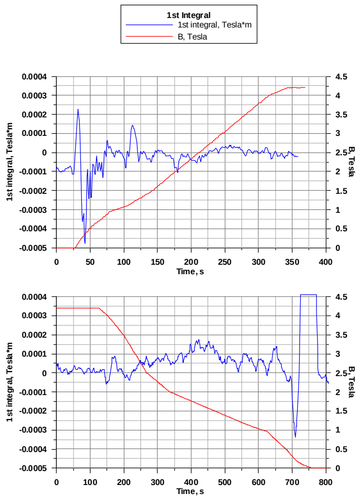

First field integral behavior during ramping field up and down.

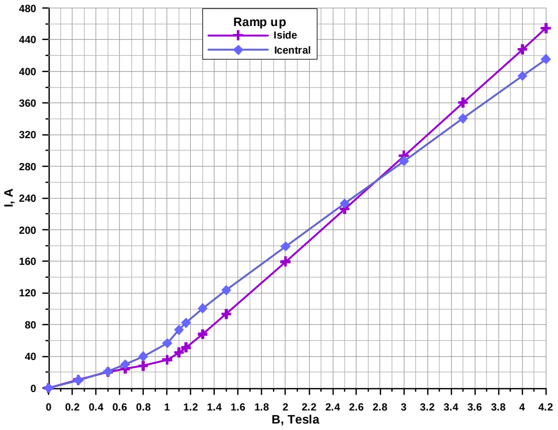

The currents Iside and Icentral for zero first field integral versus magnetic field

Thanks for your attention

Bibliography

1. Fred M. Asner “High Field superconducting magnets”, Clarendon Press, Oxford, 1999
2. Steffen, K. G. (1965). High Energy Beam Optics . Wiley.
3. K.H.Mess,P.Schmüsser,S.Wolff “Superconducting accelerator magnets”, World Scientific Publishing Co.,1996
4. Handbook of cryogenic engineering, Edited by Weisend J.G., 1998, Taylor & Francis
5. S. Prestemon,D. Dietderich, S. Marks, R. Schlueter, “NbTiand Nb3Sn Superconducting UndulatorDesigns”, Workshop on Superconducting Undulatorsand Wigglers, ESRF, July 2003.
6. E. Baynham, T. Bradshaw, Steve Carr, Y. Ivanyushenkov, J. Rochford “Superconducting undulator prototype. Status of work and the plans” , Polarised PositronUndulatorMeeting, Daresbury, 21 April 2004
7. Materials of Workshop on Superconducting Undulators & Wigglers ESRF, Grenoble, France July 1, 2003
8. Materials of The 16thPan-American Synchrotron Radiation Instrumentation Conference September 21-24, 2010 @ Argonne National Laboratory, USA
9. Materials of IDMAX2010 Insertion Devices for Rings and Linacs Workshop, Lund, November 9-10, 2010